Do hydrodynamically assisted binary collisions lead to orientational ordering of microswimmers?

Norihiro Oyama,[1] John Jairo Molina,[1] and Ryoichi Yamamoto[1]

[1]*Department of Chemical Engineering, Kyoto University, Kyoto 615-8510, Japan*

(Dated: February 22, 2017)

We have investigated the onset of collective motion in systems of model microswimmers, by performing a comprehensive analysis of the binary collision dynamics using three dimensional direct numerical simulations (DNS) with fully resolved hydrodynamics. From this data, we have constructed a simplified binary collision model (BCM) which accurately reproduces the collective behavior obtained from the DNS for most cases. Thus, we show that global alignment can mostly arise solely from binary collisions. Although the agreement between both models (DNS and BCM) is not perfect, the parameter range in which notable differences appear is also that for which strong density fluctuations are present in the system (where pseudo-sound mound can be observed[1]).

PACS numbers:

arXiv:1606.03839v2 [physics.flu-dyn] 21 Feb 2017

I. INTRODUCTION

Active matter encompasses a vast range of systems, from microorganisms at the microscopic scale, to humans and other mammals at the macroscopic scale[2, 3]. These active systems can show various nontrivial collective behaviors [1, 4–9]. Especially striking is the global ordering in the absence of any external field or leading agents[10–14]. In order to validate the various scenarios that have been proposed to explain such phenomena, it is important to develop model systems which can be well-controlled experimentally and efficiently simulated. For this purpose, micro-swimmers, such as microbes and self-propelled Janus particles, have been extensively used. It is well known that the hydrodynamic interactions play a very important role in determining the dynamics of dispersions of such microswimmers[15]. While the experimental realizations can be rather complicated, simple computational models exist which allow for direct numerical calculations, such that the full hydrodynamic effects can be accurately represented. Indeed, several simulation works on model microswimmer dispersions have recently been performed in order to study the role of hydrodynamics[1, 14, 16–19]. Of particular interest for our current work is the study by Evans *et al.*[14], who investigated the conditions under which polar ordering appears. They found that the ordering does not depend strongly on the volume fraction of swimmers, but rather on the type and strength of the swimming. The fact that we observe ordering in very dilute dispersions suggests that the mechanisms leading to the collective alignment do not depend on the volume fraction, and could be explained by considering only binary collisions. Thus, in this work we investigate the onset of polar ordering by performing a detailed analysis of the collision data obtained from three dimensional (3D) simulations of swimmer suspensions with full hydrodynamics. First, we have extended the study of Evans' *et al.*, by performing direct numerical simulations (DNS) of bulk suspensions over a larger set of parameters. We have confirmed that the volume fraction dependence is weak if the volume fraction is small enough (if it is high, order/disorder phase transition takes place). Second, by simulating binary particle collision events with varying collision geometries, we have gathered comprehensive information on the changes in swimming direction that a particle feels when it undergoes a collision. If we look at changes in the relative angles of two particles after the collisions, the results show different tendencies depending on the sign of α. Pullers tend to exhibit disalignment when the incoming relative angle is small, while pushers exhibit disalignment at intermediate values. Furthermore, using this binary collision data, we have constructed a simple binary collision model (BCM) and used it to study the collective alignment of many particle systems as a function of swimming type. The BCM successfully reproduced the emergence of the polar order except for dispersions of intermediate pullers for which a strong clustering behavior is reported[1, 19].

II. SIMULATION METHODS

A. The Squirmer Model

In this work, the squirmer model was used to describe the swimmers[20, 21]. Squirmers are particles with modified stick boundary conditions at their surface which are responsible for the self-propulsion. The general form is given as an infinite expansion of both radial and tangential velocity components, but for simplicity the radial terms are usually neglected and the infinite sum is truncated to second order[22]. For spherical particles, the surface velocity is given by

$$\boldsymbol{u}^s(\theta) = B_1 \left(\sin\theta + \frac{\alpha}{2} \sin 2\theta \right) \hat{\boldsymbol{\theta}}, \tag{1}$$

where $\hat{\boldsymbol{\theta}}$ and $\hat{\boldsymbol{r}}$ (we use a caret to denote unit vectors) are the tangential and radial unit vectors for a given point at the surface of the particle and $\theta = \cos^{-1}(\hat{\boldsymbol{r}} \cdot \hat{\boldsymbol{e}})$ is the

polar angle (since the system is axisymmetric around the swimming direction $\hat{\boldsymbol{e}}$, the azimuthal angle does not appear). The steady-state swimming velocity is determined only by the coefficient of the first mode B_1, and the ratio of the first two modes $\alpha = B_2/B_1$ determines the type and strength (stresslet) of the swimming. When α is negative, the squirmers are pushers, and generate extensile flow fields, and when it is positive, they are pullers and generate contractile flow fields. For the special case when $\alpha = 0$, we refer to the swimmers as a neutral swimmer which is accompanied by a potential flow. We call α the swimming parameter in the following.

B. Smoothed Profile Method

In order to solve for the dynamics of squirmers swimming in a viscous host fluid, the coupled equations of motion for the fluid and the solid particles needs to be considered. Particles follow the Newton-Euler equations of motion:

$$\begin{aligned} \dot{\boldsymbol{R}}_i &= \boldsymbol{V}_i & \dot{\boldsymbol{Q}}_i &= \mathrm{skew}(\boldsymbol{\Omega}_i)\cdot\boldsymbol{Q}_i \\ M_\mathrm{p}\dot{\boldsymbol{V}}_i &= \boldsymbol{F}_i^\mathrm{H} + \boldsymbol{F}_i^\mathrm{C} & \boldsymbol{I}_\mathrm{p}\cdot\dot{\boldsymbol{\Omega}}_i &= \boldsymbol{N}_i^\mathrm{H} \end{aligned} \tag{2}$$

where i is the particle index, $\boldsymbol{R}_i$ the position, $\boldsymbol{Q}_i$ the orientational matrix, and skew($\boldsymbol{\Omega}_i$) the skew symmetric matrix of the angular velocity $\boldsymbol{\Omega}_i$. The hydrodynamic force $\boldsymbol{F}_i^\mathrm{H}$ and torque $\boldsymbol{N}_i^\mathrm{H}$ are computed assuming momentum conservation to guarantee proper coupling between the fluid and the particles. To satisfy the excluded volume effect, we also introduced a repulsive interaction between particles, $\boldsymbol{F}_i^\mathrm{C}$, as a truncated Lennard-Jones potential with (36-18) powers. The time evolution of the fluid flow field is governed by the Navier-Stokes equation with the incompressible condition:

$$\boldsymbol{\nabla}\cdot\boldsymbol{u}_\mathrm{f} = 0 \tag{3}$$

$$\rho_\mathrm{f}\left(\partial_t + \boldsymbol{u}_\mathrm{f}\cdot\nabla\right)\boldsymbol{u}_\mathrm{f} = \nabla\cdot\boldsymbol{\sigma}_\mathrm{f} \tag{4}$$

$$\boldsymbol{\sigma}_\mathrm{f} = -p\boldsymbol{I} + \eta_\mathrm{f}\left\{\nabla\boldsymbol{u}_\mathrm{f} + (\nabla\boldsymbol{u}_\mathrm{f})^t\right\} \tag{5}$$

where ρ_f is the fluid mass density, η_f the shear viscosity, and $\boldsymbol{\sigma}_\mathrm{f}$ is the Newtonian stress tensor. To couple these equations efficiently, we have used the Smoothed Profile Method (SPM), which enables us to calculate the solid/fluid two-phase dynamics on fixed grids with full hydrodynamic interactions[23–26]. In the SPM, the sharp interface between the solid and fluid domains is replaced by a diffuse one with finite width ξ, and the solid phase is represented by a smooth and continuous profile function ϕ_p. This profile function takes a value of 1 in the solid domain, and 0 in the fluid domain. By introducing the smoothed profile function, we can define a total velocity field, $\boldsymbol{u}$, which includes both fluid and particle velocities, and is defined over the entire computational domain, as:

$$\begin{aligned} \boldsymbol{u} &= (1-\phi)\,\boldsymbol{u}_\mathrm{f} + \phi\boldsymbol{u}_\mathrm{p}, \\ \phi\boldsymbol{u}_\mathrm{p} &= \sum_i \phi_i\left[\boldsymbol{V}_i + \boldsymbol{\Omega}_i\times\boldsymbol{R}_i\right], \end{aligned} \tag{6}$$

where, $(1-\phi)\,\boldsymbol{u}_\mathrm{f}$ is the contribution from the fluid, $\phi\boldsymbol{u}_\mathrm{p}$ from the particle motion. The time evolution of the total flow field $\boldsymbol{u}$ obeys:

$$\begin{aligned} \boldsymbol{\nabla}\cdot\boldsymbol{u} &= 0, \\ \rho_\mathrm{f}\left(\partial_t + \boldsymbol{u}\cdot\nabla\right)\boldsymbol{u} &= \nabla\cdot\boldsymbol{\sigma}_\mathrm{f} + \rho_\mathrm{f}\left(\phi\boldsymbol{f}_\mathrm{p} + \boldsymbol{f}_\mathrm{sq}\right) \end{aligned} \tag{7}$$

where $\phi\boldsymbol{f}_\mathrm{p}$ is the body force necessary to maintain the rigidity of particles, and $\boldsymbol{f}_\mathrm{sq}$ is the force due to the active squirming motion. This method drastically reduces the computational cost.

III. RESULTS

A. Bulk Polar Order

To start, we used the SPM to carry out DNS studies of bulk swimmer dispersion in 3D at varying volume fraction φ and swimming type α. We use a cubic system of linear dimension of 64Δ, with Δ the grid spacing. The viscosity and the mass density of the host fluid, μ, ρ_f are set to one, such that the unit of time is $t_0 = \rho_f\Delta^2/\mu$. The particle diameter σ and the interface thickness ξ are 4Δ and 2Δ respectively. We used a random initial configuration for the particle positions and orientations, and varied the number of particles N_p from 500 to 4000, which correspond to a range of volume fraction $0.06 \lesssim \varphi \lesssim 0.5$. To quantify the degree of collective alignment, we calculate the polar order parameter P[14, 19]

$$P = \left\langle \frac{1}{N_\mathrm{p}}\left|\sum_i^{N_\mathrm{p}} \hat{\boldsymbol{e}}_i\right|\right\rangle, \tag{8}$$

where $\hat{\boldsymbol{e}}_i$ is the swimming direction of particle i, N_p the number of particles and angular brackets denote an average over time (after steady state has been reached). Typical simulation snapshots for disordered ($P \simeq 0$) and ordered ($P \simeq 1$) systems are given in Fig. 1(a). We note that even for a completely random distribution of orientations, the polar order defined by Eq. (8) will not be exactly 0, and will depend slightly on the number of particles, as $P_0 = 1/\sqrt{N_\mathrm{p}}$, where P_0 represents the polar order value below which we can consider the system is in an isotropic phase.

The polar order parameter P is a function of only the volume fraction of particles φ and the swimming parameter α[14]. First, we investigated α dependency. The results are illustrated in Fig. 1(b), for volume fractions $\varphi = 6\%$ ($N_\mathrm{p} = 500$),13% ($N_\mathrm{p} = 1000$) and 38% ($N_\mathrm{p} = 3000$). All the results show a similar tendency

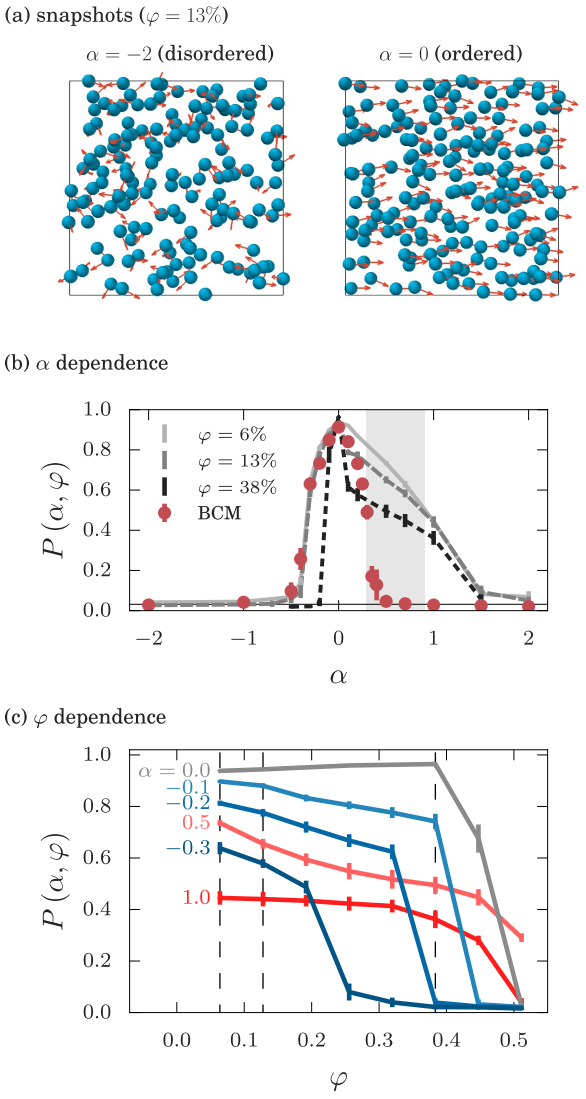

FIG. 1: (a) Simulation snapshots for disordered ($\alpha = -2$) and ordered ($\alpha = 0$) states. The arrows give the direction of motion, and only a subset of the particles have been drawn. (b) The α dependency of the polar order $P(\alpha, \varphi)$ for $\varphi = 6\%$ (solid line), 13% (light dashed line) and 38% (dark dashed line). Results for the simplified binary collision model are given as circles. (c) The φ dependency of $P(\alpha, \varphi)$ for several values of α. Dashed vertical lines indicate the volume fractions of 6, 13 and 38% used in (a) and (b).

and are in agreement with preceding woks[14, 19]: P has a maximum at $\alpha = 0$, independent of φ, and decreases with increasing value of $|\alpha|$. In addition, the P for pushers decays faster than that of pullers as the magnitude of α is increased. For non-pusher $\alpha \geq 0$, the volume fraction dependence of P is not very large and at least the qualitative ordering tendency is the same; but for weak pushers (for example $\alpha \approx -0.3$), we observe a significant drop in the value of P, or an order/disorder phase transition when the volume fraction increases. The volume fraction dependence can be seen clearly in Fig. (1c), where we have plotted the values of P over the entire volume fraction range for six different swimmers ($\alpha = -0.3, -0.2, -0.1, 0, 0.5, 1$). Evans *et al.* have previously reported such a volume fraction dependence for $\alpha = 1$ [14]. To understand the dependence of P on the swimming type α, in particular the different behaviors seen for pushers and pullers, it is useful to compare them against the results obtained for neutral swimmers $\alpha = 0$, which show the highest degree of alignment. As seen in Figure1 (c), the order parameter for $\alpha = 0$ shows two distinct regimes: for $\varphi \lesssim 0.4$ there is little variation; for $\varphi \gtrsim 0.4$ there is a drastic drop in the order parameter to $P = 0$ (P_0). The same behavior is observed for pushers, although both of the degree of ordering and the critical volume fraction φ_c (where the order parameter falls to zero) are both reduced (higher $|\alpha|$ resulting in lower P and φ_c). In contrast, pullers show a gradual decrease only in the degree of order depending on $|\alpha|$. Interestingly, intermediate pullers ($\alpha = 0.5$) maintain a non-zero order parameter over the entire volume fraction range we have considered (all other systems giving $P \approx P_0$ at the highest φ). We believe this anomalous behavior for the intermediate pullers can be related to the strong clustering behavior that gives rise to density inhomogeneities[1, 19]. Note that because the number of particles are sufficiently large (even for the system with the smallest volume fraction which corresponds to $N_p = 500$, the value of P_0 is less than 0.05), the decays in P are not related to the fact that we use different values of N_p.

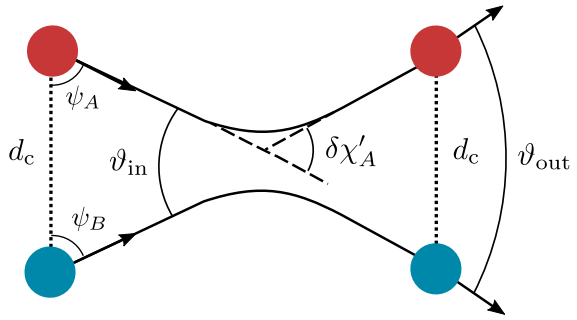

FIG. 2: Schematic representation of the collision geometry.

B. Binary Collision Analysis

Taking into account the fact that at low volume fractions, two body interactions are dominant, we can expect that the observed polar order in bulk is due to binary collisions. To verify this, we first conducted an intensive analysis on the binary collision of squirmers with varying

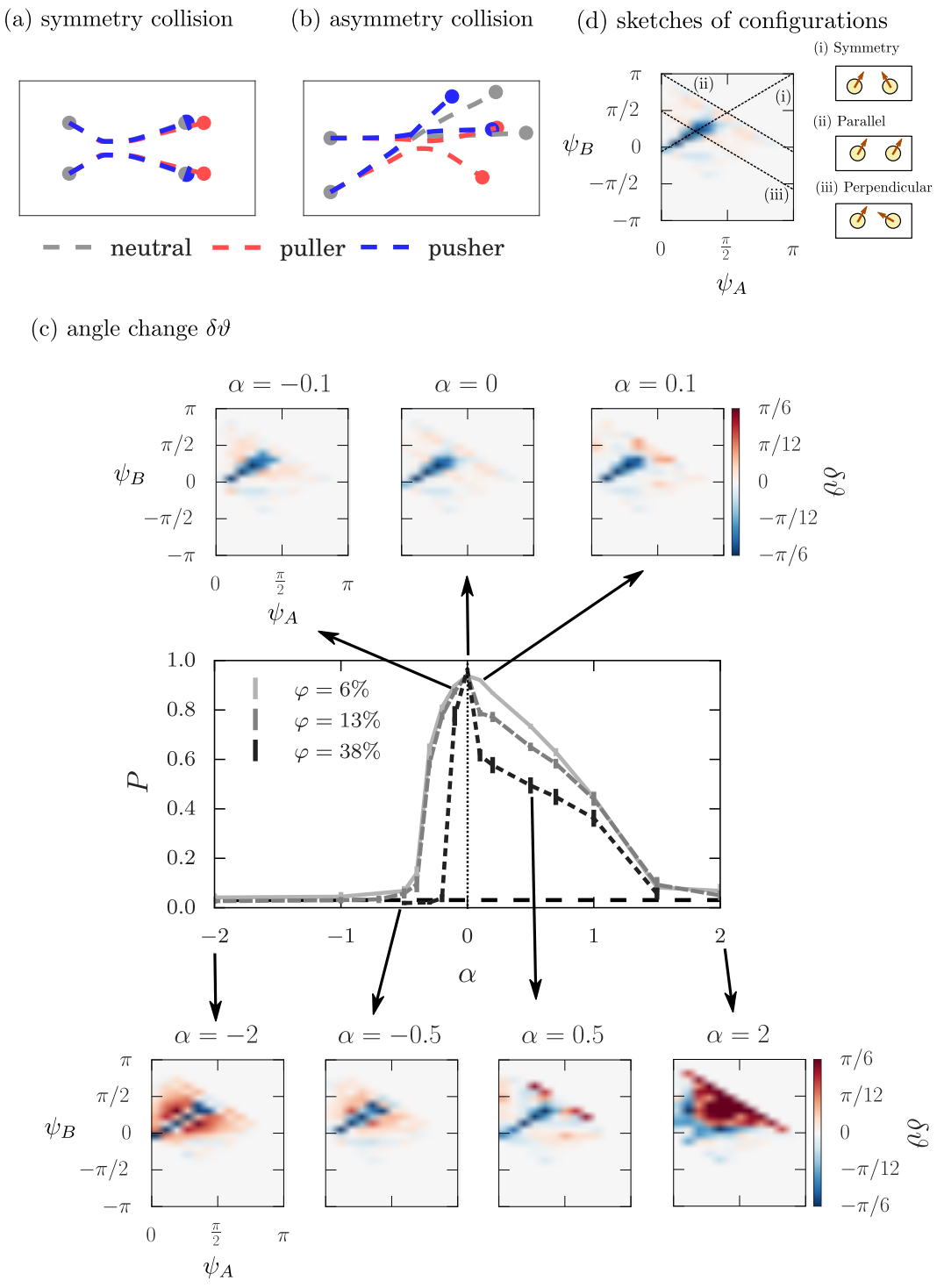

FIG. 3: (a-b) Typical trajectories of collisions of neutral swimmer ($\alpha = 0$; colored as gray), pullers ($\alpha = 0.5$; red) and pushers ($\alpha = -0.5$; blue) for (a) a symmetric collision and (b) an asymmetric one. (c) Change in the relative angle between the particles during collisions, $\delta\vartheta = \vartheta_{\rm out} - \vartheta_{\rm in}$, as a function of the initial orientations, $\psi_{\rm A}$ and $\psi_{\rm B}$. Results of bulk polar order measurement are also shown ($\varphi = 6, 13$ and 38%). In intensity maps, red colors mean positive values or the disalignment effect and blue colors negative or the aligning effect. (d) Sketches for the characteristic configurations in the intensity maps in (c).

values of α. Then, we tried to construct a simplified binary collision model (BCM) using the data obtained by this analysis. We note that a similar binary collision analysis for pullers has been done by Ishikawa *et al.*[27]. We have extended their work to pushers and neutral swimmers and made direct comparison between the BCM and the bulk DNS results. For this, we have carried out 3D DNS for a pair of particles with various collision geometries and α values. Given the symmetry of the problem, the two particles will move in a 2D plane (defined by the two orientation vectors). We considered collisions of two particles labeled A and B. The precise parametrization we have used to describe the collision is given in Fig. 2, where three sets of angles have been defined, ψ_j, $\delta\chi_j$ ($j \in \{A, B\}$ is the particle label) and $\vartheta_{\mathrm{in/out}}$. The initial configuration of the system is specified by ψ_j, the angles between the direction of motion and the center-to-center distance vector at the initial state. These angles determine whether particles start swimming towards or away from each other. The information for the change in the swimming direction of each particle is given by $\delta\chi_j$. Then, the relative orientation of particles when the collision event starts/ends is represented by $\vartheta_{\mathrm{in/out}}$. Due to the long-range nature of the hydrodynamic interactions, there is no unique way to define a "collision" between particles. Therefore, we define a characteristic distance d_c that is the threshold distance under which particles are considered to be colliding: a collision event has started when the distance between the two particles becomes less than d_c, and it lasts until the distance exceeds this value (see Figure 2). Thus, d_c should be large enough that hydrodynamic interactions can be neglected when the distance between the particles exceeds d_c.

The parameters for the binary collision is determined as follows. The initial particle distance was set to $d_0 = 16\Delta = 4\sigma$, and the collision threshold to $d_c = 15\Delta$. The value of d_c is determined to be big enough so that we can safely ignore the hydrodynamic interactions if the particle-particle distance is greater than d_c (above this value, particles hardly change their orientations). The value of d_0 is determined so that swimmers have obtained their steady state velocity when the inter-particle distance becomes d_c. The initial geometry was varied by changing ψ_j in intervals of $\pi/12$, for $0 \le \psi_A \le \pi$ and $-\pi \le \psi_B \le \pi$. To take into account the symmetry of the system, we label one of the particles (A) as a reference particle, and take $\psi_A \ge 0$, while ψ_B is defined as

$$\psi_B = \mathrm{sign}\left(\mathcal{P}_{AB}\cdot\hat{\boldsymbol{e}}_A\right)\mathrm{sign}\left(\mathcal{P}_{AB}\cdot\hat{\boldsymbol{e}}_B\right)\left|\arccos\left(\hat{\boldsymbol{r}}_{AB}\cdot\hat{\boldsymbol{e}}_B\right)\right| \tag{9}$$

where $\boldsymbol{r}_{AB} = \boldsymbol{r}_B - \boldsymbol{r}_A$, $\mathcal{P}_{AB}$ is the projection operator (with $\mathcal{I}$ the identity operator)

$$\mathcal{P}_{AB} = \mathcal{I} - \hat{\boldsymbol{r}}_{AB}\hat{\boldsymbol{r}}_{AB} \tag{10}$$

and $\mathrm{sign}(x) = 1$ for $x \ge 0$ and $\mathrm{sign}(x) = -1$ for $x < 0$. As mentioned above, we use a caret to denote unit vectors. Thus, ψ_B is defined as positive if both particles are swimming towards the same side with respect to the center-to-center line between particles. We note that only combinations of ψ_j which meet $\hat{\boldsymbol{e}}_{AB}\cdot\hat{\boldsymbol{r}}_{AB} < 0$ can lead to "collisions", where $\boldsymbol{e}_{AB} = \hat{\boldsymbol{e}}_B - \hat{\boldsymbol{e}}_A$. Three-dimensional simulations for the binary collision were performed using the same system parameters as for the bulk simulations presented above.

The results of the binary collision analysis are summarized in Fig. 3. Fig. 3(a) and (b) show typical trajectories and Fig. 3(c) shows changes in the relative angle between the swimming direction of the two particles after the collisions, $\delta\vartheta = \vartheta_{\mathrm{out}} - \vartheta_{\mathrm{in}}$. In the following, we define a symmetric collision as a collision in which $\psi_A = \psi_B$ (Fig. 3(a)). Intensity maps show the values of $\delta\vartheta$ as a function of the initial angles, ψ_j. In Fig. 3(d), the schematic representations of three characteristic initial configurations are shown: (i) symmetric, (ii) parallel, (iii) perpendicular. Although the parallel configuration does not lead to a collision, it is useful to identify the corresponding region in the intensity plots shown in Fig. 3(c). The values of the polar order in bulk are again shown to make the connection between the bulk and binary collision dynamics clear. As shown in Fig. 3 (a) and (b), different values of α lead to different particle trajectories, resulting in different patterns for $\delta\vartheta$ (Fig. 3 (c)). Note that for symmetric collisions, the trajectories of neutral swimmers and pushers are quite close to each other (Fig. 3 (a)). The results of $\delta\vartheta$ in systems of pushers and pullers can be easily understood by considering their deviation from the results for neutral swimmers ($\alpha = 0$). The neutral swimmers show strong aligning behaviors only when the collision is symmetric, and just small absolute values of $\delta\vartheta$ otherwise. If we look at the results for pullers ($\alpha > 0$), we can perceive that, in the case of $\alpha = 0.1$, disalignment effects are detected at small relative incoming angles. Such disalignment effects becomes stronger with the increase in the absolute value of α, as shown in the subplots for $\alpha = 0.5, 2$. On the other hand, in the cases of pushers ($\alpha < 0$), disalignment effects are seen at relatively large incoming angles. For pushers, as well as for pullers, the increase in the absolute value of α leads to stronger disalignment effect. In this way, measuring only $\delta\vartheta$, we can observe different tendencies between pushers and pullers. These tendencies seem to be a consequence of the complicated hydrodynamic interactions, and it is impossible to understand intuitively from the view point of the flow field which a single swimmer generates.

To implement a simple binary collision model using the collision data obtained from the DNS, it is necessary to measure the changes in the single particle orientations, $\delta\chi_j$. For this, from the comprehensive DNS data for binary collisions, we have determined $\delta\chi_j$ for all the collisions, as

$$\delta\chi_j = \arcsin\left(\hat{\boldsymbol{z}}_\chi\cdot\left(\hat{\boldsymbol{e}}_j^{\mathrm{in}}\times\hat{\boldsymbol{e}}_j^{\mathrm{out}}\right)\right), \tag{11}$$

where the superscript "in/out" refers to the value at the

moment when a collision starts/ends, $\hat{\boldsymbol{z}}_\chi = \frac{\hat{\boldsymbol{e}}_j^{\rm in} \times \hat{\boldsymbol{e}}_{j'}^{\rm in}}{|\hat{\boldsymbol{e}}_j^{\rm in} \times \hat{\boldsymbol{e}}_{j'}^{\rm in}|}$ and j' refers to the particle which is colliding with particle j.

Finally, in order to investigate whether the polar order seen in bulk systems can be explained only by binary collisions, we constructed a binary collision model (BCM). Here, we have necessarily introduced two simplifications. First, we assume 2D systems. And second, we consider only binary collisions, and use the statistics of collision angles obtained from the present DNS. Because we are assuming very dilute system such that the information of the position doesn't matter anymore, the particles have only the information about the orientations. Under these simplifications, we calculated the polar order of the system of BCM using the following simple algorithm. At each step of the simulation, we randomly choose two particles (let's say particles i and i'). The selected particles will experience a "collision", which will change their orientations according to the statistics obtained from the binary collision analysis:

$$\begin{aligned} \chi_i\left(s+1\right) &= \chi_i\left(s\right) + \delta\chi_i, \\ \chi_{i'}\left(s+1\right) &= \chi_{i'}\left(s\right) + \delta\chi_{i'}, \\ \chi_k\left(s+1\right) &= \chi_k\left(s\right), \end{aligned} \tag{12}$$

where subscript k stands for the particles which are not selected to collide. The values $\delta\chi_i$ and $\delta\chi_{i'}$ are random numbers generated according to the conditional probability distribution when the relative incoming angle $\vartheta_{\rm in}$ is given: $P\left(\delta\chi_i, \delta\chi_{i'} | \vartheta_{\rm in}\left(i,i'\right)\right)$, where $\delta\vartheta\left(i,i'\right)$ means the relative incoming angle between particles i and i'. The conditional probability distribution $P\left(\delta\chi_i, \delta\chi_{i'} | \vartheta_{\rm in}\left(i,i'\right)\right)$ is determined by using the results of the binary collision analysis presented above. Because there is the information about only the orientation in the BCM, the orientation update algorithm is based only on the relative incoming angle $\bar{\vartheta}_{\rm in}$, and does not depend on the collision parameter (which cannot be defined in this model system) or other geometrical information. Such stochastic collisions will be repeated until the steady state is achieved. In this work, we used $N_{\rm p} = 1000$ for BCM. No noise term is included. After a sufficiently large number of collisions, the system reaches a steady state, with a constant polar order. We conducted calculations using this BCM for various values of α, while keeping the value of $N_{\rm p} = 1000$ the same. The results for these simulations are plotted in Fig. (1b) as red circles, lines representing the results from the bulk DNS with $\varphi = 6\%, 13\%$, and 38%. The results from the BCM and those from the bulk DNS under dilute condition ($\varphi = 6\%$) are in good agreement with each other for non-pullers ($\alpha \leq 0$). This indicates that the appearance of polar order can be understood just in terms of binary collision events for non-pullers. For pullers, we see a growing deviation: the larger α becomes, the larger the deviation becomes. For $\alpha \geq 0.4$, even qualitatively the results are different: in the BCM, the order is collapsed. The shaded gray region in the figure marks the parameter range in which we have observed strong clustering in bulk systems[1]; it is precisely in this regions where the results do not coincide with the BCM. This can be seen as indirect evidence for the importance of multi-body interactions for the collective alignment of intermediate pullers. In pipes, we also observed similar indirect evidence for the importance of the many body interactions for the polar order formation in systems of intermediate pullers[28]. There, we reported that the polar order in the system of intermediate pullers is suppressed when the pipe size becomes small, while such a order/disorder transition cannot be observed for other types of swimmers. We consider such a phase transition indicates that intermediate pullers require clusters with a certain characteristic size to maintain the polar order. In small pipes, they are unable to form such clusters and seem to fail maintaining the order. Though several efforts have been dedicated to verify the importance of binary collisions to explain the polar order formation for various systems both experimentally and numerically [29–33], the presented work is the first successful attempt to conduct such analysis considering full hydrodynamics.

IV. CONCLUSION

Using DNS for squimer dispersions, we have investigated the emergence of polar ordering and its dependency on the particle volume fraction φ and swimming strength α. In agreement with a previous work[14], we see that the volume fraction dependence is rather weak, and the ordering depends mostly on α when φ is small enough, while at a large value of volume fraction, we observe an order/disorder phase transition. Still, we observed novel volume fraction dependencies for $|\alpha| < 1$. In particular, intermediate pullers show no decay of the polar order even at a very high volume fraction, at which all other swimmers show a decay. We believe this anomalous behavior at such a high volume fraction reflects the already-known strong clustering characteristics[1, 19]. On the other hand, weak pushers show a decay of the polar order even at small volume fractions.

We conducted a detailed analysis of the binary collision dynamics of two swimmers and looked at the changes in the relative orientation of two swimmers after the collisions. The results show different qualitative disaligning tendencies between pusher and puller: pullers show disaligning effects at small relative incoming angles while pushers exhibit at relatively large angles. The absolute value of α changes only the magnitude of disalignment, and the tendency is determined by the sign. Such an analysis also enabled us to construct a simple binary collision model which is able to reproduce the polar ordering seen in the bulk DNS for pushers and neutral swimmers. Thus, it seems binary collisions are enough to explain the appearance of long range polar ordering for these types of swimmers. We note that intermediate pullers exhibit a clear discrepancy between the DNS results and the BCM; however, this occurs in the parameter range where strong

clustering behavior is also observed. This can be seen as indirect evidence that in intermediate puller systems, clustering due to many body interactions plays an important role. In other words, the origin of the polar order formation can be different, depending on the specific type of swimming. In particular, the mechanism responsible for the clustering of intermediate pullers is still an open question.

V. ACKNOWLEDGEMENT

We thank M. Tarama, H. Ito, K. Ishimoto and Simon K. Schnyder for enlightening discussions. This work was supported by the Japan Society for the Promotion of Science (JSPS) KAKENHI Grant No. 26247069 and also by a Grant-in-Aid for Scientific Research on Innovative Areas "Dynamical ordering of biomolecular systems for creation of integrated functions"(No. 16H00765) from the Ministry of Education, Culture, Sports, Science, and Technology of Japan. We also acknowledge the supporting program for interaction-based initiative team studies (SPIRITS) of Kyoto University.

[1] N. Oyama, J. J. Molina, and R. Yamamoto, Physical Review E **93**, 043114 (2016).
[2] T. Vicsek and A. Zafeiris, Physics Reports **517**, 71 (2012).
[3] M. C. Marchetti, J. F. Joanny, S. Ramaswamy, T. B. Liverpool, J. Prost, M. Rao, and R. A. Simha, Reviews Of Modern Physics **85**, 1143 (2013).
[4] E. Lushi, H. Wioland, and R. E. Goldstein, Proceedings of the National Academy of Sciences **111**, 9733 (2014).
[5] B. Ezhilan, M. J. Shelley, and D. Saintillan, Physics of Fluids **25**, 070607 (2013).
[6] H. Chaté, F. Ginelli, G. Grégoire, F. Peruani, and F. Raynaud, The European Physical Journal B **64**, 451 (2008).
[7] S. Bazazi, J. Buhl, J. J. Hale, M. L. Anstey, G. A. Sword, S. J. Simpson, and I. D. Couzin, Current Biology **18**, 735 (2008).
[8] J. Buhl, D. J. T. Sumpter, I. D. Couzin, J. J. Hale, E. Despland, E. R. Miller, and S. J. Simpson, Science **312**, 1402 (2006).
[9] A. Zöttl and H. Stark, Journal of Physics: Condensed Matter **28**, 253001 (2016).
[10] M. Ballerini, N. Cabibbo, R. Candelier, A. Cavagna, E. Cisbani, I. Giardina, V. Lecomte, A. Orlandi, G. Parisi, A. Procaccini, M. Viale, and V. Zdravkovic, in *Proceedings of the National Academy of Sciences* (2008) pp. 1232–1237.
[11] D. Volfson, S. Cookson, J. Hasty, and L. S. Tsimring, in *Proceedings of the National Academy of Sciences* (2008) pp. 15346–15351.
[12] R. Lukeman, Y.-X. Li, and L. Edelstein-Keshet, in *Proceedings of the National Academy of Sciences* (2010) pp. 12576–12580.
[13] V. Schaller, C. Weber, C. Semmrich, E. Frey, and A. R. Bausch, Nature **467**, 73 (2010).
[14] A. A. Evans, T. Ishikawa, T. Yamaguchi, and E. Lauga, Physics of Fluids **23** (2011).
[15] S. Rafaï, L. Jibuti, and P. Peyla, Physical Review Letters **104**, 098102 (2010).
[16] K. Kyoya, D. Matsunaga, Y. Imai, T. Omori, and T. Ishikawa, Physical Review E **92**, 063027 (2015).
[17] A. Zöttl and H. Stark, Physical Review Letters (2014).
[18] G.-J. Li and A. M. Ardekani, Physical Review E **90**, 013010 (2014).
[19] F. Alarcon and I. Pagonabarraga, Molecular Simulations of Complex Systems **185 IS -**, 56 (2013).
[20] M. J. Lighthill, Communications on Pure and Applied Mathematics **5**, 109 (1952).
[21] J. R. Blake, Journal of Fluid Mechanics **46**, 199 (1971).
[22] T. Ishikawa and T. J. Pedley, Journal of Fluid Mechanics **588**, 437 (2007).
[23] Y. Nakayama and R. Yamamoto, Physical Review E **71**, 036707 (2005).
[24] K. Kim, Y. Nakayama, and R. Yamamoto, Physical Review Letters **96**, 208302 (2006).
[25] Y. Nakayama, K. Kim, and R. Yamamoto, The European Physical Journal E **26**, 361 (2008).
[26] J. J. Molina, Y. Nakayama, and R. Yamamoto, Soft Matter **9**, 4923 (2013).
[27] T. Ishikawa, M. P. Simmonds, and T. J. Pedley, Journal of Fluid Mechanics **568**, 119 (2006).
[28] N. Oyama, J. J. Molina, and R. Yamamoto, arXiv.org (2016), 1612.00135v1 .
[29] Y. Katz, K. Tunstrøm, C. C. Ioannou, C. Huepe, and I. D. Couzin, in *Proceedings of the National Academy of Sciences* (2011) pp. 18720–18725.
[30] T. Hanke, C. A. Weber, and E. Frey, Physical Review E **88**, 052309 (2013).
[31] K.-D. N. T. Lam, M. Schindler, and O. Dauchot, New Journal of Physics **17**, 1 (2015).
[32] R. Suzuki, C. A. Weber, E. Frey, and A. R. Bausch, Nature Physics **11**, 839 (2015).
[33] T. Hiraoka, T. Shimada, and N. Ito, Physical Review E **94**, 062612 (2016).